PCCP

ROYAL SOCIETY OF CHEMISTRY

PAPER

View Article Online
View Journal | View Issue

Cite this: *Phys. Chem. Chem. Phys.*, 2022, **24**, 16586

Extended quasiparticle approach to non-resonant and resonant X-ray emission spectroscopy

Kaoru Ohno * and Tsubasa Aoki

Received 28th February 2022,
Accepted 20th June 2022

DOI: 10.1039/d2cp00988a

rsc.li/pccp

The initial states of the secondary processes of X-ray emission spectroscopy (XES) and resonant inelastic X-ray scattering (RIXS) are highly excited eigenstates with a deep core hole after a X-ray photoelectron spectroscopy (XPS) process and a X-ray photoabsorption spectroscopy (XAS) process, respectively, so that the XES and RIXS calculation offers a good example of extended quasiparticle theory (EQPT) (K. Ohno, S. Ono and T. Isobe, *J. Chem. Phys.*, 2017, **146**, 084108) which is applicable to any initial exited eigenstate. We apply the standard one-shot *GW* + Bethe–Salpeter equation (BSE) approach in MBPT to this problem on the basis of EQPT and analyze XES and RIXS spectra for CH_4, NH_3, H_2O, and CH_3OH molecules. We also suggest a simpler approach only using the *GW* calculation without solving the BSE to compute the XES and RIXS energies, although it cannot give the spectral intensity. Moreover, according to extended Kohn–Sham theory (T. Nakashima, H. Raebiger and K. Ohno, *Phys. Rev. B*, 2021, **104**, L201116), we give a justification and comment of applying the method relying on time-dependent density functional theory as well as the one-shot *GW* + BSE approach to this problem.

1 Introduction

Recent advances in synchrotron[1] and in-house[2] X-ray sources have accelerated the use of powerful analytical tools involving an excitation of a core electron.[3,4] While X-ray photoelectron spectroscopy (XPS) and X-ray photoabsorption spectroscopy (XAS) use the primary process of exciting one electron from a core level up to, respectively, above and below the vacuum level, (non-resonant) X-ray emission spectroscopy (XES) and resonant inelastic X-ray scattering (RIXS) involve the secondary processes, where X-ray radiative recombination of a valence electron and a core hole takes place after the XPS core-level ionization and the XAS core-electron excitation, respectively. XES and RIXS have been recognized as new experimental techniques for chemical analyses which can give important information of valence electrons in the presence of a deep core hole.[5,6] However, since the initial states in the secondary processes of XES and RIXS are highly excited eigenstates with a deep core hole, which is created in the preceding XPS and XAS processes, a first-principle calculation using the *GW* + Bethe–Salpeter equation (BSE) method[7] in many-body perturbation theory (MBPT) or time-dependent density functional theory (TDDFT)[8] for XES and RIXS is a big challenge. This situation is different from XPS and XAS, whose initial states are the ground state. Below, we confine our discussion to XES and RIXS only.

In order to obtain the transition energies and the intensities of XES spectra, Besley *et al.*[9] applied configuration interaction singles (CIS), TDDFT, and equation of motion – coupled cluster singles & doubles (EOM-CCSD) methods. Concerning the X-ray fluorescence photon energies, the TDDFT results with BLYP and B3LYP exchange–correlation functionals showed large deviations from the experimental data due to the self-interaction error, but the use of a short-range-corrected functional improved the results. Their CIS, TDDFT(B3LYP), and EOM-CCSD results with the 6-3111G** basis set for the carbon K-edge XES spectrum of a CH_3OH molecule showed, however, three peaks only in contrast to the experimental spectrum[10] showing five peaks. Recently, Besley refined the TDDFT result and obtained five peaks using B3LYP[11] or CAM-B3LYP[12] with the cc-pCVQZ basis set, but still an empirical shift by −6.3 eV or −5.7 eV was required to fit to the experimental XES spectrum. (A larger shift by +10.9 eV was required for a direct comparison between the Kohn–Sham eigenvalues and the experimental XES spectrum.[12]) In the present paper, we focus this problem from a different point of view on the basis of exact theories, *i.e.*, extended quasiparticle theory (EQP) by Ohno *et al.*[13] and extended Kohn–Sham (EKS) theory which was quite recently established by Nakashima *et al.*[14] There are also several other reports on XES using TDDFT.[15–18] Recently, Cruz *et al.*[19,20] used TDDFT for the RIXS analysis.

On the other hand, in order to treat XES or RIXS with the Green's function method in MBPT, Vinson *et al.*[21,22] performed a standard one-shot *GW* (G_0W_0) calculation and solve the BSE for valence excitations only. Their initial state for XES is the neutral N electron ground state, not the true $N-1$ electron state. Therefore, they had to introduce an empirical parameter to compare their results with experiments. However, according to EQP theory,[13]

Department of Physics, Yokohama National University, 79-5 Tokiwadai, Hodogaya-ku, Yokohama 240-8501, Japan. E-mail: ohno@ynu.ac.jp

one can start calculation of the GW + BSE method of MBPT from an arbitrary excited eigenstate. That is, EQP theory allows us to set the initial state to be the $N-1$ (or N) electron excited state with a deep core hole, where one electron is emitted from the core level to the vacuum (empty) level. This theory can remove the difficulty to compute XES and RIXS spectra with MBPT, which is a clear novelty. Indeed, we have recently succeeded in calculating the XES spectra of several small molecules (CH_4, NH_3, H_2O, CH_3OH) using the G_0W_0 + BSE method of MBPT without introducing any empirical parameter.[23] In our approach, the initial state of the GW + BSE method is the core-excited state.

The purpose of the present paper is to give a justification of using MBPT and TDDFT for XES and RIXS and discuss the problem lying in the existing methodologies. Here, we apply the G_0W_0 + BSE method to the XES and RIXS analysis of CH_4, NH_3, H_2O, and CH_3OH molecules and discuss the accuracy of the resulting spectra. Moreover, according to extended Kohn–Sham theory,[14] we give a justification and comment of applying the method relying on TDDFT as well as the one-shot GW + BSE approach to this problem. Based on this theory, we discuss the proper problem of the XES and RIXS calculations.

In what follows, we assume, as usual, that the initial state of the XES and RIXS secondary processes is an excited eigenstate of the total Hamiltonian. However, some non-equilibrium effect may occur in the experimental situation. For example, we have totally ignored the effect of molecular vibration, which is sometimes experimentally observed in the XES and RIXS spectra.[24] So, we have to say that we use a time-independent approximation and totally ignore dynamical effect. However, for the dynamics, we have successfully performed a TDGW molecular dynamics simulation for the excited state CO* + H → HCO reaction[25] on the basis of EQP theory. Another research using the non-equilibrium Green's function technique[26,27] has been performed by Spataru *et al.*[28] and by Perfetto and Stefanucci.[29] Such studies should be extended to the X-ray related dynamics[30] in the future.

The rest of this paper is organized as follows. First, we will briefly review EQP and EKS theories in Section 2. Computational details and results of our RIXS calculation based on EQP theory are given, respectively, in Sections 3 and 4. Discussions are given in Section 5, where a simpler approach only using the GW calculation without solving the BSE is suggested, and finally Section 6 concludes the paper.

2 Theory

2.1 EQP theory

Here we briefly review the keypoint of extended quasiparticle (EQP) theory.[13] First, let us derive the equation satisfied by the EQP wave functions and the EQP energies. The Hamiltonian H is given by $H = H^{(1)} + H^{(2)}$ with the one-body part

$$H^{(1)} = \hat{T} + \hat{v} = \sum_s \int \hat{\psi}_s^\dagger(\mathbf{r}) h^{(1)}(\mathbf{r}) \hat{\psi}_s(\mathbf{r}) \mathrm{d}\mathbf{r}, \qquad h^{(1)}(\mathbf{r}) = -\frac{\hbar^2}{2m}\nabla^2 + v(\mathbf{r}) \tag{1}$$

and the two-body part

$$H^{(2)} = \frac{1}{2}\sum_{ss'} \int \hat{\psi}_s^\dagger(\mathbf{r}) \hat{\psi}_{s'}^\dagger(\mathbf{r}') V(\mathbf{r}-\mathbf{r}') \hat{\psi}_{s'}(\mathbf{r}') \hat{\psi}_s(\mathbf{r}) \mathrm{d}\mathbf{r}\mathrm{d}\mathbf{r}', \tag{2}$$

where $\hat{\psi}(\mathbf{r})$, $\hat{\psi}_s^\dagger(\mathbf{r})$ are annihilation and creation operators at position and spin coordinates $(\mathbf{r}, s)$, $V(\mathbf{r}-\mathbf{r}') = e^2/4\pi\varepsilon_0|\mathbf{r}-\mathbf{r}'|$ is the Coulomb interaction, and $v(\mathbf{r}) = -\sum_I Z_I V(\mathbf{r}-\mathbf{R}_I)$ is the nuclear potential. The commutation relation between $\hat{\psi}(\mathbf{r})$ and H is given by

$$[\hat{\psi}_s(\mathbf{r}), H] = h^{(1)}\hat{\psi}_s(\mathbf{r}) + \sum_{s'} \int \hat{\psi}_{s'}^\dagger(\mathbf{r}') V(\mathbf{r}'-\mathbf{r}) \hat{\psi}_{s'}(\mathbf{r}') \hat{\psi}_s(\mathbf{r}) \mathrm{d}\mathbf{r}'. \tag{3}$$

Let $|\Psi_\lambda^{M\pm1}\rangle$ and $|\Psi_\gamma^M\rangle$ be the $(M\pm1)$- and M-electron eigenstates of the Hamiltonian H, and $E_\lambda^{M\pm1}$ and E_γ^M be the corresponding energy eigenvalues. Then, by sandwiching eqn (3) with $\langle\Psi_\mu^{M-1}|$ and $|\Psi_\gamma^M\rangle$ or with $\langle\Psi_\gamma^M|$ and $|\Psi_\nu^{M+1}\rangle$, we derive

$$\left(E_\gamma^M - E_\mu^{M-1}\right)\left\langle \Psi_\mu^{M-1}\middle|\hat{\psi}_s(\mathbf{r})\middle|\Psi_\gamma^M\right\rangle = h_s^{(1)}(\mathbf{r})\left\langle \Psi_\mu^{M-1}\middle|\hat{\psi}_s(\mathbf{r})\middle|\Psi_\gamma^M\right\rangle + \sum_{s'}\int V(\mathbf{r}'-\mathbf{r})\left\langle \Psi_\mu^{M-1}\middle|\hat{\psi}_{s'}^\dagger(\mathbf{r}')\hat{\psi}_{s'}(\mathbf{r}')\hat{\psi}_s(\mathbf{r})\middle|\Psi_\gamma^M\right\rangle \mathrm{d}\mathbf{r}', \tag{4a}$$

$$\left(E_\nu^{M+1} - E_\gamma^M\right)\left\langle \Psi_\gamma^{M}\middle|\hat{\psi}_s(\mathbf{r})\middle|\Psi_\nu^{M+1}\right\rangle = h_s^{(1)}(\mathbf{r})\left\langle \Psi_\gamma^{M}\middle|\hat{\psi}_s(\mathbf{r})\middle|\Psi_\nu^{M+1}\right\rangle + \sum_{s'}\int V(\mathbf{r}'-\mathbf{r})\left\langle \Psi_\gamma^{M}\middle|\hat{\psi}_{s'}^\dagger(\mathbf{r}')\hat{\psi}_{s'}(\mathbf{r}')\hat{\psi}_s(\mathbf{r})\middle|\Psi_\nu^{M+1}\right\rangle \mathrm{d}\mathbf{r}'. \tag{4b}$$

Here, the second term in the right-hand side (r.h.s.) of eqn (4) is conventionally rewritten as

$$\sum_{s'}\int V(\mathbf{r}'-\mathbf{r})\left\langle \Psi_\mu^{M-1}\middle|\hat{\psi}_{s'}^\dagger(\mathbf{r}')\hat{\psi}_{s'}(\mathbf{r}')\hat{\psi}_s(\mathbf{r})\middle|\Psi_\gamma^M\right\rangle \mathrm{d}\mathbf{r}' = \int \Sigma_s\left(\mathbf{r},\mathbf{r}', E_\gamma^M - E_\mu^{M-1}\right)\left\langle \Psi_\mu^{M-1}\middle|\hat{\psi}_s(\mathbf{r}')\middle|\Psi_\gamma^M\right\rangle \mathrm{d}\mathbf{r}', \tag{5a}$$

$$\sum_{s'}\int V(\mathbf{r}'-\mathbf{r})\left\langle \Psi_\gamma^{M}\middle|\hat{\psi}_{s'}^\dagger(\mathbf{r}')\hat{\psi}_{s'}(\mathbf{r}')\hat{\psi}_s(\mathbf{r})\middle|\Psi_\nu^{M+1}\right\rangle \mathrm{d}\mathbf{r}' = \int \Sigma_s(\mathbf{r},\mathbf{r}', E_\nu^{M+1} - E_\gamma^M)\left\langle \Psi_\gamma^{M}\middle|\hat{\psi}_s(\mathbf{r}')\middle|\Psi_\nu^{M+1}\right\rangle \mathrm{d}\mathbf{r}', \tag{5b}$$

by introducing the energy-dependent self-energy $\Sigma_s(\mathbf{r},\mathbf{r}';\varepsilon_\lambda)$. Since both identities (5a) and (5b) hold simultaneously, they should be an equivalent identity. In fact, if we replace M, μ and γ with $M+1$, γ and ν in eqn (5a), we obtain eqn (5b). This means that both equations should hold for arbitrary M, γ, μ and ν. This is the reason that MBPT can be applicable to an arbitrary excited eigenstate as an initial state. Indeed the full Green's function formulation of MBPT can be reproduced by using the Brillouin–Winger perturbation theory,[13] which is certainly applicable to any excited eigenstate without doubt. Now, defining EQP energies as

$$\varepsilon_\mu = E_\gamma^M - E_\mu^{M-1}, \quad \varepsilon_\nu = E_\nu^{M+1} - E_\gamma^M, \tag{6}$$

and EQP wave functions as

$$\phi_\mu(\mathbf{r},s)=\langle\Psi_\mu^{M-1}|\hat{\psi}(\mathbf{r})|\Psi_\gamma^M\rangle,\quad \phi_\nu(\mathbf{r},s)=\langle\Psi_\gamma^M|\hat{\psi}(\mathbf{r})|\Psi_\nu^{M+1}\rangle, \tag{7}$$

we successfully derive EQP equations

$$h^{(1)}(\mathbf{r})\phi_\mu(\mathbf{r},s)+\int\Sigma_s(\mathbf{r},\mathbf{r}',\varepsilon_\mu)\phi_\mu(\mathbf{r}',s)\mathrm{d}\mathbf{r}'=\varepsilon_\mu\phi_\mu(\mathbf{r},s), \tag{8a}$$

$$h^{(1)}(\mathbf{r})\phi_\nu(\mathbf{r},s)+\int\Sigma_s(\mathbf{r},\mathbf{r}',\varepsilon_\nu)\phi_\nu(\mathbf{r}',s)\mathrm{d}\mathbf{r}'=\varepsilon_\nu\phi_\nu(\mathbf{r},s) \tag{8b}$$

from eqn (5a) and (5b).

EQP energies defined by eqn (6) directly correspond to the photoemission (PE) and inverse photoemission (IPE) energies associated with the initial excited eigenstate $|\Psi_\gamma^M\rangle$, and EQP wave functions defined by eqn (11) describe the created hole and electron (particle) distribution in the corresponding PE/IPE process. However, EQP wave functions are not orthogonal to each other and their norm is less than one.[31–33] They are even not linearly independent.[34] Therefore, there are, in principle, infinite number of occupied (occ) EQP wave functions $\phi_\mu(\mathbf{r},s)$ even for the finite M-electron system, as there are infinite number of $(M-1)$-electron states $|\Psi_\mu^{M-1}\rangle$. This implies that the electron spin density

$$\begin{aligned}\rho_s(\mathbf{r}) &= \left\langle\Psi_\gamma^M\middle|\hat{\psi}_s^\dagger(\mathbf{r})\hat{\psi}_s(\mathbf{r})\middle|\Psi_\gamma^M\right\rangle\\ &= \sum_\mu^{\mathrm{occ}}\left\langle\Psi_\gamma^M\middle|\hat{\psi}_s^\dagger(\mathbf{r})\middle|\Psi_\mu^{M-1}\right\rangle\left\langle\Psi_\mu^{M-1}\middle|\hat{\psi}_s(\mathbf{r})\middle|\Psi_\gamma^M\right\rangle\\ &= \sum_\mu^{\mathrm{occ}}\phi_\mu^*(\mathbf{r},s)\phi_\mu(\mathbf{r},s)\\ &= \sum_\mu^{\mathrm{occ}}\left|\phi_\mu(\mathbf{r},s)\right|^2\end{aligned} \tag{9}$$

must be expressed with an infinite sum of occupied EQP wave functions even in the finite M-electron system, and makes the rigorous analysis such as in highly correlated systems difficult. This problem was, however, solved quite recently by extended Kohn–Sham theory explained in Section 2.2.

2.2 EKS theory

Extended Kohn–Sham (EKS) theory[14] solves this problem on the normalization of EQP wave functions. Multiplying both sides of eqn (8) by $e^{-i\varepsilon_\lambda t_1}$ and using the original definition $\Sigma_s(r_1,r_2;\varepsilon_\lambda)=\int\mathrm{d}(t_1-t_2)\Sigma_s(1,2)\mathrm{e}^{i\varepsilon_\lambda(t_1-t_2)}$ (numbers are abbreviations for position and time coordinates, *i.e.*, $i=(\mathbf{r}_i,t_i)$), one readily obtains the time-dependent EQP equation[35,36]

$$i\frac{\partial}{\partial t_1}\phi_\lambda(1,s)=h^{(1)}(\mathbf{r}_1)\phi_\lambda(1,s)+\int\Sigma_s(1,2)\phi_\lambda(2,s)d2, \tag{10}$$

where time-dependent EQP wave functions, $\phi_\lambda(1,s)$, are defined by

$$\phi_\mu(1,s)=\langle\Psi_\mu^{M-1}|\hat{\psi}(1)|\Psi_\gamma^M\rangle,\quad \phi_\nu(1,s)=\langle\Psi_\gamma^M|\hat{\psi}(1)|\Psi_\nu^{M+1}\rangle \tag{11}$$

using the Heisenberg operator $\hat{\psi}(1)=\mathrm{e}^{iHt_1}\hat{\psi}(\mathbf{r}_1)\mathrm{e}^{-iHt_1}$. Then, the two-time spin density matrix $\rho_s(1,2)$ is introduced as

$$\begin{aligned}\rho_s(1,2) &\equiv \left\langle\Psi_\gamma^M\middle|\hat{\psi}_s^\dagger(2)\hat{\psi}_s(1)\middle|\Psi_\gamma^M\right\rangle\\ &= \sum_\mu^{\mathrm{occ}}\left\langle\Psi_\gamma^M\middle|\hat{\psi}_s^\dagger(2)\middle|\Psi_\mu^{M-1}\right\rangle\left\langle\Psi_\mu^{M-1}\middle|\hat{\psi}_s(1)\middle|\Psi_\gamma^M\right\rangle\\ &= \sum_\mu^{\mathrm{occ}}\phi_\mu(1,s)\phi_\mu^*(2,s).\end{aligned} \tag{12}$$

This $\rho_s(1,2)$ coincides with the Green's function $-iG_s(1,2)$ for $t_1<t_2$ and satisfies

$$i\frac{\partial}{\partial t_1}\rho_s(1,2)=h^{(1)}(\mathbf{r}_1)\rho_s(1,2)+\int\Sigma_s(1,3)\rho_s(3,2)d3, \tag{13}$$

which is readily derived from eqn (10) by multiplying $\phi_\lambda^*(2,s)$ and summing with λ (=μ) over all occupied EQP states. Next, let us assume that $\rho_s(1,2)$ is expressed by M normalized EKS wave functions $\bar{\phi}_i(1,s)$ ($i=1,2,\ldots,M$) as

$$\rho_s(1,2)=\sum_{i=1}^M\bar{\phi}_i(1,s)\bar{\phi}_i^*(2,s). \tag{14}$$

It certainly satisfies the necessary condition for the electron spin density $\sum_s\int\rho_s(\mathbf{r}_1)\mathrm{d}\mathbf{r}_1=\sum_s\int\rho_s(1,1)\mathrm{d}\mathbf{r}_1=M$. (Note that the original ϕ_λ had norm less than 1 and infinite number of ϕ_λ were required to satisfy this necessary condition.) At each time t_1, we can introduce the dual orbitals $\tilde{\phi}_j(1,s)$ ($j=1,2,\ldots,M$), which satisfy the biorthogonality condition

$$\int\bar{\phi}_i^*(1,s)\tilde{\phi}_j(1,s)\mathrm{d}\mathbf{r}_1=\delta_{ij}\quad(i,j\le M). \tag{15}$$

Note that $\tilde{\phi}_i(1,s)$ can be made from $\bar{\phi}_i(1,s)$ by using the the Gram–Schmidt orthogonalization to all the other $M-1$ orbitals $\bar{\phi}_j^*(1,s)$ ($j\neq i$). Then, we have $\int\rho_s(1,2)\tilde{\phi}_i(2,s)\mathrm{d}\mathbf{r}_2=\bar{\phi}_i(1,s)$ for $i\le M$. Then, eqn (13) yields the equation[14]

$$i\frac{\partial}{\partial t_1}\bar{\phi}_i(1,s)=h^{(1)}(\mathbf{r}_1)\bar{\phi}_i(1,s)+\int\Sigma_s(1,2)\bar{\phi}_i(2,s)\mathrm{d}2. \tag{16}$$

Eqn (10) and (16) have exactly the same form, and thus we know that $\bar{\phi}_i(1,s)$ is equivalent to the EQP wave function $\phi_\mu(1,s)$ except for a normalization factor. Therefore, the electron spin density $\rho_s(\mathbf{r}_1)=\rho_s(1,1)$ is expressed by M normalized EQP wave functions except for normalization. Those functions are not necessarily mutually orthogonal. So far, we discussed the occupied EQP wave functions only, but a similar discussion is possible also for the empty EQP wave functions.[14]

Although there are a lot of independent excitations that are not directly associated with the PE and IPE processes in the $(M\pm1)$-electron states $|\Psi_\lambda^{M\pm1}\rangle$, they can be eliminated in the summation over all occupied (and empty) EQP states, and instead we have to accept that the EQP energies have an imaginary part, which represents the peak width and the inverse of the QP lifetime. However, according to Baym–Kadanoff's conservation laws,[37,38] we can derive the hermitized

equation[14]

$$\left[h^{(1)}+\frac{1}{2}\{\Sigma(\varepsilon_\lambda)+\Sigma^\dagger(\varepsilon_\lambda)\}\right]|\phi_\lambda\rangle=\mathrm{Re}[\varepsilon_\lambda]|\phi_\lambda\rangle, \tag{17}$$

which can be regarded as the EKS equation. Moreover, we derive[32,33]

$$\left\langle\phi_\lambda\middle|\left[1-\frac{\partial\Sigma(\omega)}{\partial\omega}\bigg|_{\omega=\varepsilon_\lambda}\right]\middle|\phi_\lambda\right\rangle=1. \tag{18}$$

Thus the operator $1-\partial\Sigma(\omega)/\partial\omega|_{\omega=\varepsilon\lambda}$ normalizes the EQP states. This normalization procedure is closely related to the Ward identity[38,39]

$$\Gamma_{q=0}(\omega)=1-\frac{\partial\Sigma(\omega)}{\partial\omega}, \tag{19}$$

which is the $q\to 0$ limit of the Ward–Takahashi identity, where $q\equiv(\mathbf{q},\omega'-\omega)$ denotes the momentum-energy transfer *via* the Coulomb interaction. In eqn (19), $\Gamma_{q=0}(\omega)$ is the vertex operator in the $q\to 0$ limit. Comparing (19) with (18), we have[14]

$$\langle\phi_\lambda|\Gamma_{q=0}(\varepsilon_\lambda)|\phi_\lambda\rangle=1. \tag{20}$$

The vertex function, which connects the dynamical interaction to a pair of Green's functions, has an effect to make the system gauge invariant by the Ward–Takahashi identity, and guarantees the local charge conservation by the continuity equation.[38,40] However, in the limit $q\to 0$, no multiple excitation is possible. Therefore, the vertex function in this limit counts the $(M\pm 1)$-electron states $|\Psi_\lambda^{M\pm1}\rangle$ with purely one electron or hole only, and has an effect to normalize the corresponding EQP wave functions to unity, ignoring all the other EQP wave functions involving multiple excitations. This is the physical meaning of eqn (20).

A simple way to normalize EQP wave functions is to multiply the Green's function by[14]

$$\begin{aligned}\Gamma^{\mathrm{ren}}_{q=0s}(\mathbf{r}_1,\mathbf{r}_2;\omega)&=\langle\mathbf{r}_1,s|\Gamma^{\mathrm{ren}}_{q=0}(\omega)|\mathbf{r}_2,s\rangle=\delta(\mathbf{r}_1-\mathbf{r}_2)f(\omega),\\ f(\omega)&=\sum_{\lambda\in\mathrm{all}}\frac{1}{\langle\phi_\lambda|\phi_\lambda\rangle}\frac{\prod_{\alpha\neq\lambda}(\omega-\varepsilon_\alpha)}{\prod_{\beta\neq\lambda}(\varepsilon_\lambda-\varepsilon_\beta)}\end{aligned} \tag{21}$$

and introduce the normalized Green's function $\bar{G}(\omega)$ as

$$\bar{G}(\omega)=\Gamma^{\mathrm{ren}1/2}_{q=0}(\omega)G(\omega)\Gamma^{\mathrm{ren}1/2}_{q=0}(\omega)=G(\omega)f(\omega). \tag{22}$$

It is proved[14] in Hedin's exact *GWΓ* formulation that the frequency integrals at each order of the expansion in terms of skeleton-diagrams equally give rise to all contributions from the poles of all Green's functions in the series, and therefore $f(\omega)\to f(\varepsilon_\lambda)$ normalizes all EQP wave functions appearing inside all Green's functions in the expansion. Therefore, one can simply normalize the EQP wave functions to unity. The only difference from the traditional DFT is that the EQP wave functions are not necessarily orthogonal to each other, because the self-energy is energy dependent. A non-orthogonality actually implies that the EQP wave functions are interacting, or correlated, in contrast to the fictitious non-interacting KS orbitals. This EKS theory is applicable to the excited states, *i.e.* the problem of the XES and RIXS studies, by relying on EQP theory explained in Section 2.1. However, the very important message here is that one has to use an accurate nonlocal self-energy in order to obtain a good result.

3 Computational details

There is also a problem of basis functions to represent the wave functions for the XES and RIXS studies. The electronic structure calculations in quantum chemistry usually use the Gaussian basis functions which are not always suited to represent highly extended states. To overcome the basis set incompleteness, we apply the all-electron mixed basis approach,[41] in which both plane waves (PWs) and numerical atomic orbitals (AOs) are used as basis functions. We have successfully applied this approach in our previous XPS[42,43] and XES[23] studies. A similar XPS study has been performed by Golze *et al.*[44] Here, we select CH_4, NH_3, H_2O, and CH_3OH molecules as target systems. There are experimental XES data for these molecules.[10,45–47] There are also experimental RIXS data for NH_3,[48] H_2O,[49] and CH_3OH.[50] We take the input coordinates of these target molecules from the PubChem3D data.[51] First, we perform the DFT calculation for the spin-polarized electron configuration for the XES and RIXS excited states with a core hole. We use the local density approximation (LDA) of Perdew–Zunger's interpolation formula[52] for the exchange–correlation functional. Second, using the resulting Kohn–Sham (KS) eigenvalues and KS orbitals, we calculate the EQP energies using the one-shot *GW* approach. In this approach, the EQP wave functions are replaced by the LDA Kohn–Sham orbitals $\phi_\lambda^{\mathrm{LDA}}(\mathbf{r},s)$, and the *GW* EQP energies ε_λ^{GW} are estimated from the LDA energy eigenvalues $\varepsilon_\lambda^{\mathrm{LDA}}$ as

$$\begin{aligned}\varepsilon_\lambda^{GW}=\varepsilon_\lambda^{\mathrm{LDA}}+Z_\lambda\sum_s\int\phi_\lambda^{\mathrm{LDA}*}(\mathbf{r},s)\Big[\Sigma_s(\mathbf{r},\mathbf{r}';\varepsilon_\lambda^{\mathrm{LDA}})\\ -\mu_{\mathrm{xc}}^{\mathrm{LDA}}(\mathbf{r})\delta(\mathbf{r}-\mathbf{r}')\Big]\phi_\lambda^{\mathrm{LDA}}(\mathbf{r}',s)\mathrm{d}\mathbf{r}\mathrm{d}\mathbf{r}'\end{aligned} \tag{23}$$

with a renormalization factor

$$Z_\lambda=\left[1-\sum_s\int\phi_\lambda^{\mathrm{LDA}*}(\mathbf{r},s)\frac{\partial\Sigma_s(\mathbf{r},\mathbf{r}';\omega)}{\partial\omega}\bigg|_{\omega=\varepsilon_\lambda^{\mathrm{LDA}}}\phi_\lambda^{\mathrm{LDA}}(\mathbf{r}',s)\mathrm{d}\mathbf{r}\mathrm{d}\mathbf{r}'\right]^{-1}. \tag{24}$$

Finally, the BSE is solved within the Tamm–Dancoff approximation.[53] In order to avoid quite heavy numerical ω integrations, the generalized plasmon pole (GPP) model[54] is applied to the dynamical screened Coulomb interaction in the correlation term of the *GW* self-energy[54] and the direct term of BSE Hamiltonian.[7] The computational conditions such as unit cell parameters, cutoff energies for PWs, the Fock exchange Σ_x and the correlation term $\Sigma_c(\omega)$ (here, the self-energy $\Sigma(\omega)$ is decomposed as $\Sigma(\omega)=\Sigma_x+\Sigma_c(\omega)$), and the number of levels are listed in Table 1. For AOs, we use minimal basis, *i.e.*, 1s, $2p_x$, $2p_y$, $2p_z$ for C, N, O and 1s for H. (AOs are confined inside nonoverlapping atomic spheres.) All calculations in this paper use periodic boundary conditions. So, in order to treat the

Table 1 Molecules, unit cell parameters (simple cubic), cutoff energies for plane waves (E_{PW}^{cutoff}), exchange (E_x^{cutoff}) and correlation (E_c^{cutoff}), and the number of levels used in the *GW* + BSE calculations

Molecule	Cell parameter (Å)	E_{PW}^{cutoff} PW (Ry)	E_x^{cutoff} exchange (Ry)	E_c^{cutoff} correlation (Ry)	Number of levels
CH_4	$a = b = c = 12.0$	44.2	122.8	11.1	2000
NH_3	$a = b = c = 10.0$	63.7	223.9	15.9	2000
H_2O	$a = b = c = 10.0$	63.7	223.9	15.9	2500
CH_3OH	$a = b = c = 14.0$	38.1	114.2	11.1	2500

isolated systems, we use the spherical cut technique for the Coulombic interactions.[55] The radius of Coulomb truncation is the half of the side length of the simple cubic unit-cell, and the molecular size should be smaller than this radius.

4 Results

First we show the one-shot *GW* (G_0W_0) results. Initial state has a core hole at C1s for CH_4 and CH_3OH, N1s for NH_3, and O1s for H_2O, corresponding to the K-edge XES/RIXS spectra of carbon, nitrogen, and oxygen atoms. The other electron configuration is the same as the neutral ground state in XES (X). In contrast, in RIXS (R), one electron, which has the same spin as the removed core electron, is added to the LUMO level. This corresponds to the lowest-energy singlet exciton with a core hole induced by the X-ray absorption. These states are generated within the LDA. Contributions to the one-shot *GW* calculation are listed in Tables 2–5. In these tables, asterisk (*) attached onto ε^{GW} values indicates occupied levels, and ε^{GW} values without asterisk are empty levels. Note that the *GW* energy ε^{GW} is not the simple addition of $\Sigma_x + \Sigma_c - \mu_{xc}^{LDA}$ because of the existence of the prefactor, *i.e.* the renormalization factor Z_λ in eqn (23). We see from these tables that, for all molecules, there are interesting correlations between the up spin and down spin EQP states and between the XES (X*n*) and RIXS (R*n*). For example, ε^{LDA} and ε^{GW} have similar values between up and down spins at the same level, when both spin states are simultaneously occupied or

Table 2 Contributions to the one-shot *GW* calculation for XES (X) and RIXS (R) of CH_4. ε^{LDA} and μ_{xc}^{LDA} are the LDA eigenvalue and the expectation value of the LDA exchange–correlation potential; Σ_x and Σ_c are, respectively, the exchange and correlation parts of the self-energy; and ε^{GW} is the *GW* extended quasiparticle energy. Asterisk (*) attached onto ε^{GW} values indicates occupied levels. This table lists the data for single-particle levels (X*n*, R*n*) only

	Up spin (eV)					Down spin (eV)				
Process/level	ε^{LDA}	μ_{xc}^{LDA}	Σ_x	Σ_c	ε^{GW}	ε^{LDA}	μ_{xc}^{LDA}	Σ_x	Σ_c	ε^{GW}
X1 (C1s)	−331.6	−60.9	−103.5	10.4	−359.1*	−300.6	−28.9	−3.2	−10.5	−287.8
R1 (C1s)	−325.7	−60.8	−103.5	12.4	−348.3*	−295.2	−29.4	−3.4	−12.6	−285.8
X2	−29.3	−17.5	−27.5	3.1	−35.5*	−28.2	−15.9	−25.0	2.8	−33.8*
R2	−23.6	−17.4	−27.3	4.5	−29.7*	−22.6	−16.0	−25.3	6.9	−23.7*
X3–5	−21.0	−16.5	−22.5	0.8	−25.9*	−20.4	−15.3	−21.1	0.6	−25.2*
R3–5	−15.3	−16.4	−22.3	2.3	−18.2*	−14.8	−15.3	−21.1	2.2	−17.5*
X6	−6.6	−6.3	−2.8	−0.9	−4.0	−6.3	−5.6	−2.1	−0.8	−3.6
R6	−2.5	−4.7	−1.6	−2.0	−1.5	−2.8	−4.7	−5.6	−1.2	−4.6*
X7–9	−5.5	−9.0	−4.0	−1.1	−1.7	−5.2	−8.4	−3.6	−1.0	−1.5
R7–9	−1.2	−4.7	−1.4	−1.8	0.2	−1.5	−4.3	−2.0	−1.1	−0.6

Table 3 Contributions to the one-shot *GW* calculation for XES (X) and RIXS (R) of NH_3. ε^{LDA} and μ_{xc}^{LDA} are the LDA eigenvalue and the expectation value of the LDA exchange–correlation potential; Σ_x and Σ_c are, respectively, the exchange and correlation parts of the self-energy; and ε^{GW} is the *GW* extended quasiparticle energy. Asterisk (*) attached onto ε^{GW} values indicates occupied levels. This table lists the data for single-particle levels (X*n*, R*n*) only

	Up spin (eV)					Down spin (eV)				
Process/level	ε^{LDA}	μ_{xc}^{LDA}	Σ_x	Σ_c	ε^{GW}	ε^{LDA}	μ_{xc}^{LDA}	Σ_x	Σ_c	ε^{GW}
X1 (N1s)	−453.1	−71.3	−121.3	12.0	−485.8*	−417.3	−34.6	−4.3	−12.2	−401.8
R1 (N1s)	−446.1	−71.2	−121.2	14.4	−473.5*	−410.8	−35.1	−4.5	−14.6	−399.1
X2	−34.7	−20.4	−32.0	3.7	−41.9*	−33.4	−18.5	−29.1	3.3	−40.0*
R2	−27.9	−20.3	−31.9	5.6	−33.7*	−26.7	−18.6	−29.6	6.8	−29.3*
X3–4	−24.0	−19.0	−26.0	0.9	−29.7*	−23.3	−17.6	−24.2	0.7	−28.7*
R3–4	−17.3	−18.9	−25.8	2.6	−20.9*	−16.7	−17.6	−24.1	2.3	−20.4*
X5	−19.9	−20.2	−28.1	1.5	−25.8*	−18.7	−18.3	−25.5	1.2	−24.3*
R5	−13.4	−20.0	−27.6	3.1	−17.2*	−12.4	−18.2	−25.2	2.8	−16.9*
X6	−8.0	−7.7	−3.5	−1.0	−4.8	−7.7	−7.1	−2.8	−0.9	−4.5
R6	−2.9	−5.7	−2.0	−2.1	−1.5	−3.4	−5.9	−7.1	−1.0	−5.4*
X7–8	−6.4	−9.6	−4.5	−1.0	−2.5	−6.1	−9.0	−4.0	−1.0	−2.2
R7–8	−1.3	−5.7	−2.1	−2.0	0.1	−1.8	−5.9	−3.1	−1.2	−0.4
X9	−3.7	−3.0	−1.0	−0.5	−1.6	−3.6	−2.9	−1.0	−0.4	−2.1
R9	−0.5	−2.4	−0.5	−1.2	−0.0	−0.9	−2.8	−1.1	−1.0	−0.3

Table 4 Contributions to the one-shot *GW* calculation for XES (X) and RIXS (R) of H_2O. ε^{LDA} and μ_{xc}^{LDA} are the LDA eigenvalue and the expectation value of the LDA exchange–correlation potential; Σ_x and Σ_c are, respectively, the exchange and correlation parts of the self-energy; and ε^{GW} is the *GW* extended quasiparticle energy. Asterisk (*) attached onto ε^{GW} values indicates occupied levels. This table lists the data for single-particle levels (X*n*, R*n*) only

	Up spin (eV)					Down spin (eV)				
Process/level	ε^{LDA}	μ_{xc}^{LDA}	Σ_x	Σ_c	ε^{GW}	ε^{LDA}	μ_{xc}^{LDA}	Σ_x	Σ_c	ε^{GW}
X1 (O1s)	−594.1	−82.0	−139.7	12.0	−634.6*	−553.9	−41.0	−5.8	−12.1	−533.6
R1 (O1s)	−585.9	−81.9	−139.7	14.5	−620.5*	−546.2	−41.5	−6.0	−14.6	−530.0
X2	−40.9	−23.9	−37.7	4.3	−49.7*	−39.7	−21.6	−34.2	3.9	−47.2*
R2	−32.9	−23.8	−37.6	7.5	−37.7*	−31.5	−21.7	−34.8	6.8	−37.1*
X3	−27.8	−22.2	−30.0	1.3	−34.3*	−26.9	−20.4	−28.0	1.0	−33.0*
R3	−19.8	−22.1	−30.1	3.1	−24.0*	−19.2	−20.5	−28.0	2.6	−24.5*
X4	−25.4	−23.5	−32.7	1.8	−32.4*	−24.1	−21.4	−30.0	1.5	−30.7*
R4	−17.6	−23.2	−32.2	3.6	−22.3*	−16.6	−21.4	−29.9	3.5	−20.8*
X5	−23.7	−24.2	−33.7	2.2	−30.6*	−22.4	−22.0	−30.8	1.8	−28.9*
R5	−16.0	−23.9	−33.2	3.9	−20.6*	−14.8	−21.9	−30.5	3.6	−19.1*
X6	−9.1	−8.8	−4.1	−0.9	−5.3	−8.8	−8.2	−3.5	−0.8	−4.9
R6	−2.8	−6.3	−2.3	−2.0	−1.0	−3.5	−7.1	−9.0	−0.7	−5.8*
X7	−7.5	−10.3	−4.9	−0.9	−5.3	−7.2	−9.8	−4.5	−0.8	−2.8
R7	−1.2	−6.3	−2.4	−1.9	0.5	−1.9	−7.3	−4.2	−1.0	0.0
X8	−4.0	−2.9	−1.0	−0.3	−2.4	−3.9	−2.8	−1.0	−0.3	−2.3
R8	−0.6	−2.6	−0.8	−1.0	0.1	−0.9	−2.7	−1.2	−0.8	−0.2
X9	−3.9	−2.9	−1.0	−0.3	−2.3	−3.8	−2.7	−0.9	−0.3	−2.3
R9	−0.3	−2.0	−0.3	−0.9	−0.4	−0.7	−2.7	−1.0	−0.7	0.1

Table 5 Contributions to the one-shot *GW* calculation for XES (X) and RIXS (R) of CH_3OH. ε^{LDA} and μ_{xc}^{LDA} are the LDA eigenvalue and the expectation value of the LDA exchange–correlation potential; Σ_x and Σ_c are, respectively, the exchange and correlation parts of the self-energy; and ε^{GW} is the *GW* extended quasiparticle energy. Asterisk (*) attached onto ε^{GW} values indicates occupied levels. This table lists the data for single-particle levels (X*n*, R*n*) only

	Up spin (eV)					Down spin (eV)				
Process/level	ε^{LDA}	μ_{xc}^{LDA}	Σ_x	Σ_c	ε^{GW}	ε^{LDA}	μ_{xc}^{LDA}	Σ_x	Σ_c	ε^{GW}
X1 (O1s)	−515.2	−78.8	−132.1	11.1	−551.4*	−515.3	−78.8	−132.1	11.1	−551.4*
R1 (O1s)	−509.4	−78.8	−132.1	13.0	−540.9*	−509.4	−78.9	−132.2	13.0	−541.0*
X2 (C1s)	−333.1	−60.8	−103.6	10.7	−360.5*	−301.9	−28.8	−3.2	−10.9	−289.4
R2 (C1s)	−326.7	−60.8	−103.5	12.6	−350.3*	−295.9	−29.1	−3.3	−12.8	−286.1
X3	−34.2	−20.7	−32.5	5.0	−40.1*	−33.9	−20.6	−32.3	5.1	−39.7*
R3	−28.3	−20.7	−32.5	6.7	−32.7*	−28.0	−20.7	−32.6	6.9	−32.7*
X4	−27.8	−18.5	−28.2	3.1	−33.8*	−26.9	−17.1	−26.1	2.8	−32.5*
R4	−21.7	−18.4	−28.0	4.8	−25.8*	−21.0	−17.2	−26.3	5.0	−24.3*
X5	−22.2	−17.5	−23.8	1.4	−26.8*	−21.8	−16.9	−23.2	1.3	−26.3*
R5	−16.2	−17.5	−23.7	2.9	−19.1*	−15.9	−17.1	−23.4	3.0	−18.7*
X6	−21.7	−16.7	−23.2	1.4	−26.5*	−21.1	−15.7	−21.9	1.2	−25.8*
R6	−15.6	−16.7	−23.0	2.8	−18.7*	−15.7	−15.2	−21.9	2.6	−18.2*
X7	−21.0	−18.6	−24.1	1.1	−25.2*	−20.5	−17.6	−23.1	1.0	−24.7*
R7	−15.0	−18.4	−23.9	2.5	−17.6*	−14.7	−17.5	−23.1	2.5	−17.3*
X8	−16.8	−19.4	−26.1	1.7	−21.5*	−16.7	−19.1	−25.8	1.7	−21.4*
R8	−11.1	−19.2	−25.8	3.0	−14.1*	−11.1	−19.0	−25.5	3.0	−14.1*
X9	−14.6	−19.7	−26.7	2.2	−19.1*	−14.6	−19.6	−26.6	2.1	−19.1*
R9	−8.9	−19.5	−26.4	3.5	−11.7*	−9.0	−19.5	−26.9	3.5	−11.8*
X10	−7.4	−13.7	−7.5	−1.5	−2.9	−7.1	−11.4	−5.8	−1.4	−3.0
R10	−2.3	−6.6	−2.7	−2.1	−0.7	−2.6	−6.3	−7.4	−1.0	−4.4*
X11	−6.5	−9.9	−5.2	−1.2	−3.1	−6.1	−9.0	−4.4	−1.1	−2.7
R11	−1.8	−9.3	−4.8	−2.1	0.3	−1.8	−6.4	−3.3	−1.4	−0.3
X12	−5.8	−9.0	−4.1	−1.1	−2.3	−5.5	−8.3	−3.5	−1.1	−1.9
R12	−5.6	−1.2	−2.2	−1.7	0.2	−1.4	−4.6	−2.1	−1.0	−0.1
X13	−5.7	−9.1	−4.1	−1.1	−2.1	−5.4	−8.5	−3.6	−1.1	−1.8
R13	−1.1	−4.6	−1.6	−1.5	0.2	−1.4	−5.3	−2.5	−1.3	−0.0

empty, while they have quite different values when up spin is occupied and down spin is empty or *vice versa*. Moreover, we notice that the expectation values of the LDA exchange–correlation potential (μ_{xc}^{LDA}) and the exchange and correlation parts of the self-energy (Σ_x and Σ_c) are almost the same (at most 2 eV difference) between X*n* and R*n*. This means that the main difference between X*n* and R*n* in the *GW* energy ε^{GW} comes from the LDA energy eigenvalue ε^{LDA}. We will discuss this point later in Section 5.

Next, the RIXS spectra obtained by solving the BSE are shown in Fig. 1 and in Fig. 2, respectively, for NH_3 and CH_3OH. The calculated XES and RIXS fluorescence photon energies are

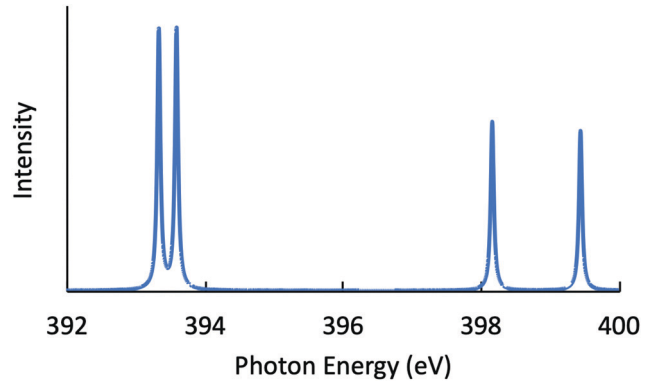

Fig. 1 Calculated RIXS spectrum for NH_3.

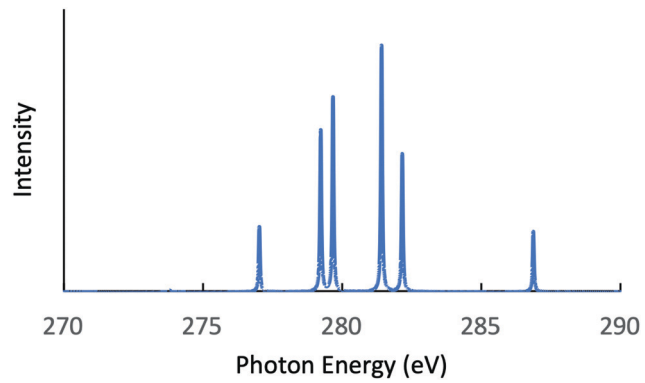

Fig. 2 Calculated RIXS spectrum for CH_3OH.

Table 6 XES and RIXS fluorescence photon energies obtained by solving the BSE after the *GW* calculation for the EQP energies, which are listed in Tables 2–5. Available experimental values[10,45–50] are listed together

		XES (eV)		RIXS (eV)	
Molecule	State	Calc.	Exp.	Calc.	Exp.
CH_4	S_1	277.5	276.4[a]	280.8	—
	S_2	277.5	276.4[a]	280.8	—
	S_3	277.5	276.4[a]	280.8	—
	S_4	—	—	285.3	—
NH_3	S_1	390.5	388.6[b]	393.4	389.0[e]
	S_2	390.5	388.6[b]	393.4	389.0[e]
	S_3	396.1	395.0[b]	398.2	392.5[e]
	S_4	—	—	399.4	394.3[e]
H_2O	S_1	521.8	520.8[c]	524.4	522.3[f]
	S_2	525.7	524.8[c]	528.5	524.3[f]
	S_3	528.1	526.6[c]	531.4	526.3[f]
	S_4	—	—	532.5	526.5[f]
CH_3OH	S_1	270.8	275.2[d]	273.8	274.3[g]
	S_2	274.6	277.0[d]	277.0	276.7[g]
	S_3	277.1	279.4[d]	279.2	279.0[g]
	S_4	277.8	281.2[d]	279.7	279.3[g]
	S_5	279.5	282.5[d]	281.4	281.0[g]
	S_6	280.2	282.8[d]	282.2	281.4[g]
	S_7	—	—	286.9	287.0[g]

[a] Ref. 45. [b] Ref. 46. [c] Ref. 47. [d] Ref. 10. [e] Ref. 48. [f] Ref. 49. [g] Ref. 50.

listed in Table 6 together with the experimental data.[10,45–50] There are three excitonic states S_1–S_3 for XES and four excitonic states S_1–S_4 for RIXS in the case of CH_4, NH_3, and H_2O molecules, while there are six excitonic states for XES and seven excitonic states for RIXS in the case of a CH_3OH molecule. The XES results are slightly different from those of our previous report[23] due to the choice of different computational conditions given in Table 1. For the present XES results, the agreement with the experimental values is better than our previous report[23] for CH_4, NH_3 and H_2O (the difference between the present results and the experimental data[45–47] is 1–1.5 eV), but a bit worse for CH_3OH (the difference from the experimental data[10] is 2–4 eV). Similarly, the RIXS results well reproduce the overall experimental tendencies. In particular, the result for NH_3 (Fig. 1) reproduces the shoulder peak observed experimentally;[48] the shoulder peak D_1 of Fig. 5 in ref. 48 corresponds to the calculated peak at 398.2 eV in Fig. 1. However, our RIXS results are systematically larger by 2–3 eV from our XES results, in contrast to the experimental XES and RIXS data showing the difference at most 1.5 eV. Accordingly, our RIXS results are systematically overestimated by 2–4 eV from the available experimental data for NH_3 and H_2O.[48,49] A possible reason of this systematic deviation is discussed in the following section. Nevertheless, it is worthwhile to note that, our RIXS result for CH_3OH (Fig. 2 and Table 6) well coincides with the experimental data.[50]

5 Discussion

The EQP energy of the C1s core hole created by a XPS process, −287.8 eV, which is given in Table 2 as X1 (C1s) ε^{GW} for down spin, should coincide with the C1s XPS energy of a neutral system. So, we performed the *GW* calculation of a neutral CH_4 molecule at the ground state and obtained ε^{GW}_{C1s} for the 1 (C1s) XPS level as shown in Table 7. The resulting C1s XPS energy ε^{GW}_{C1s} = −289.4 eV is fairly close to the EQP energy −287.8 eV of the X1 C1s core hole (Table 2) with a 1.6 eV difference, which is an error caused by the approximations used and some insufficiency of the parameter set (including the supercell size), *etc.* Anyway, the error of 1.6 eV is relatively small compared to the absolute value 288 eV and acceptable. This strongly supports the validity of the present methodology.

Moreover, using an idea to calculate the photoabsorption energy only by performing the *GW* calculation for the cation of the target molecule without solving the BSE,[56] we can estimate the XES energies only from the result given in Table 7 of a

Table 7 Contributions to the one-shot *GW* calculation for neutral CH_4 at the ground state. ε^{LDA} and μ^{LDA}_{xc} are the LDA eigenvalue and the expectation value of the LDA exchange–correlation potential; Σ_x and Σ_c are, respectively, the exchange and correlation parts of the self-energy; and ε^{GW} is the *GW* quasiparticle energy. Asterisk (*) attached onto ε^{GW} values indicates occupied levels

Level	(eV)	ε^{LDA}	μ^{LDA}_{xc}	Σ_x	Σ_c	ε^{GW}
1	(C1s)	−265.6	−58.0	−96.2	10.0	−289.4*
2		−17.1	−15.5	−24.2	2.8	−22.3*
3–5	(HOMO)	−9.5	−14.0	−19.3	0.5	−13.8*
6		−0.6	−1.8	−0.6	−0.3	0.3

neutral *GW* calculation as $\varepsilon_{C1s}^{GW} - \varepsilon_{HOMO}^{GW}$ = −289.4 + 13.8 eV = 275.6 eV, which is different from the experimental XES value −276.4 eV by 0.8 eV only. This again strongly supports the validity of the present theory, although this type of calculation (as well as the above-mentioned paper[56]) does not allow us to calculate the spectral intensity. It can be used at least for the purpose of error estimation, but we think the ability is more than that. We can more positively expect that the accuracy of the involved calculation becomes better, because this is simply a standard *GW* calculation for a neutral molecule. In fact, there was a similar advantage in the spin-unpolarized calculation in cationic systems of Al, B, Na_3, and Li_3 treated in the above-mentioned paper.[56]

Similarly, for RIXS, we performed *GW* calculation for an ammonia anion NH_3^{-1} and obtained Table 8. From down spin levels, we can estimate the RIXS energies as $\varepsilon_{N1s}^{GW} - \varepsilon_n^{GW}$ = −397.3 eV − $\varepsilon_n^{GW}(n = 3\text{–}6)$ as −385.9 eV, −385.9 eV, −390.9 eV, and −396.0 eV, which can be compared with the experimental values in Table 6: −389.0 eV, −389.0 eV, −392.5 eV, and −394.3 eV. The differences between theory and experiment are, respectively, 3.1 eV, 3.1 eV, 1.6 eV, and 1.7 eV. The larger differences compared to the CH_4 XES case discussed above are probably due to the *GW* calculation for an anion, not for a neutral molecule.

As seen in the previous section, there is a systematic deviation between our XES and RIXS results. The most probable reason is the approximation used in the present calculation. The validity of the linearization of the QP equation, *i.e.*, the so-called renormalization of the one-shot *GW* approximation, is not obvious in particular for the deep core level. So, we tried to use the X1 (C1s) $\varepsilon_{C1s}^{GW(EQP)}(\uparrow, \downarrow)$ values listed in Table 2 in the argument of the self-energy $\Sigma_c(\varepsilon^{GW(EQP)})$, and reperformed a *GW* + BSE calculation for the CH_4 XES case. The resulting $\varepsilon_{C1s}^{GW(EQP)}(\uparrow, \downarrow)$ values, however, did not change at all up to one decimal place written in Table 2 even if we used the correct EQP energy in the argument of the self-energy. The difference is about 0.01 eV. So, we think the linearization does not cause any significant problem at least in the present case. In this sense, there is no oscillatory behavior in the self-energy as discussed by Mejuto-Zaera *et al.*[57] at least in the present case. In the present and previous calculations, we have used the GPP model.[54] It is known that sometimes the GPP model gives a worse result compared with the numerical ω integration. However, unfortunately, it is quite heavy to perform the numerical ω integration for the XES and RIXS studies. From a tentative calculation, we found that there is a possibility to lower the XES and RIXS energies by using the full numerical ω integration up to 1000 points corresponding to about 200 eV. Moreover, we used the Tamm–Dancoff approximation[53] in solving the BSE.

On the other hand, as seen in Tables 2–5, the main difference between XES and RIXS in the *GW* energy ε^{GW} comes from the LDA energy eigenvalue ε^{LDA}, since the expectation values of the LDA exchange–correlation potential (μ_{xc}^{LDA}) and the exchange and correlation parts of the self-energy (Σ_x and Σ_c) are almost the same between the XES and RIXS calculations. Therefore, another reason for the difference between the resulting XES and RIXS energies may lie in the LDA energy eigenvalues ε^{LDA}. The use of LDA is an approximation in particular for excited states, even though EQP theory is the exact theory and the usual way to calculate the self-energy is justified for excited states. For example, we have to be careful for a treatment of the charge neutrality in the unit cell for a cation system required in the XES calculation. In order to exclude the interaction between the unit cells, we have introduced the spherical cut technique for the Coulombic interaction.[55] In particular, in the XES calculation of + charged molecule with a deep core hole, the effect of Coulomb spherical cut and the unit-cell size may become more serious. So, we performed a LDA calculation with a slightly larger unit cell (14 Å) for the CH_4 XES case with the same cutoff energy for plane waves as listed in Table 1. Then, we obtained −331.7 eV (up spin) and −300.6 eV (down spin) for the X1 (C1s) level, which is different from the ε^{LDA} values in Table 2 by only 0.1 eV. As well, to investigate the effect of the electric dipole, we performed a similar LDA calculation with a slightly larger unit-cell (12 Å) for the NH_3 and H_2O RIXS (charge neutral) case with the same cutoff energy for plane waves as listed in Table 1. In this case, we obtained −445.8 eV (up spin) and −410.5 eV (down spin) for the R1 (N1s) level of NH_3 and −585.7 eV (up spin) and −546.0 eV (down spin) for the R1 (O1s) level of H_2O. The difference from the ε^{LDA} values in Tables 3 and 4 is 0.3 eV for NH_3 and 0.2 eV for H_2O. Therefore, the unit-cell size listed in Table 1 is almost sufficient.

Finally, we want to give a justification and comment of applying TDDFT to the XES and RIXS studies. As demonstrated in Sections 2.1 and 2.2, Kohn–Sham equation is applicable to excited states. However, as is well known, the condition to apply TDDFT for an initially excited state is that one should use the exchange–correlation kernel constructed by including the

Table 8 Contributions to the one-shot *GW* calculation for NH_3^- anion. ε^{LDA} and μ_{xc}^{LDA} are the LDA eigenvalue and the expectation value of the LDA exchange-correlation potential; Σ_x and Σ_c are, respectively, the exchange and correlation parts of the self-energy; and ε^{GW} is the *GW* quasiparticle energy. Asterisk (*) attached onto ε^{GW} values indicates occupied levels

	Up spin (eV)					Down spin (eV)				
Level	ε^{LDA}	μ_{xc}^{LDA}	Σ_x	Σ_c	ε^{GW}	ε^{LDA}	μ_{xc}^{LDA}	Σ_x	Σ_c	ε^{GW}
1 (N1s)	−373.9	−68.3	−114.0	13.8	−397.3*	−373.9	−68.3	−114.0	13.8	−397.3*
2	−18.1	−18.1	−28.1	5.0	−20.2*	−18.1	−18.1	−28.2	5.1	−20.3*
3–4	−8.3	−15.9	−21.7	2.1	−11.3*	−8.3	−15.9	−21.7	2.1	−11.4*
5	−3.5	−15.7	−21.1	1.9	−6.4*	−3.5	−15.7	−21.0	1.9	−6.4*
6	0.5	−2.3	−0.3	−1.6	0.7	0.0	−2.7	−2.8	−1.5	−1.3*

information of the wave function of the initial excited state.[8] This should not be the simple LDA kernel. From EKS theory,[14] the true kernel should be the hermitized self-energy in MBPT, and, from EQP theory,[13] it is applicable to any excited eigenstate of the many-body Hamiltonian. This means that, even with hybrid functional such as B3LYP, the difference between the correct self-energy and the hybrid functional may cause a systematic error in the XES and RIXS calculations. It would be important to use a more elaborate functional, which imitates the important characteristic of the true self-energy.

6 Conclusion

In this paper, we have demonstrated the validity of applying the Green's function method based on many-body perturbation theory (MBPT) to the XES and RIXS studies. The important point is that one can rely on extended quasiparticle (EQP) theory[13] and extended Kohn–Sham theory,[14] which enable one to treat an arbitrary excited eigenstate as an initial state. From this point of view, we have given a justification and comment of applying TDDFT to the XES and RIXS studies. Though Kohn–Sham equation is applicable to excited states, the exchange–correlation kernel must be dependent on the initial state according to TDDFT.[8] From EKS theory,[14] the true kernel should be the hermitized self-energy in MBPT, and, from EQP theory,[13] it is applicable to any excited eigenstate of the many-body Hamiltonian. This means that, even with hybrid functional such as B3LYP, the difference between the correct self-energy and the hybrid functional may cause a systematic error in the XES and RIXS calculations. It would be important to use a more elaborate functional, which imitates the important characteristic of the true self-energy. This is, however, left for a future study.

We have explicitly applied the one-shot *GW* + Bethe–Salpeter equation (BSE) method to the XES and RIXS calculations of CH_4, NH_3, H_2O, and CH_3OH molecules, which include the chemically important K-edge XES/RIXS spectra of carbon, nitrogen, and oxygen atoms in the soft X-ray regime. Our results give the fluorescence photon energies of XES and RIXS in reasonable agreement with the experimental data, although there appear some deviations between our XES and RIXS results. We infer these errors from several approximations, such as the plasmon-pole model,[54] the Tamm–Dancoff approximation[53] or one-shot methods. So, the numerical ω integration and the self-consistent *GW* calculations will be desirable for more accurate investigations.

In Section 5, we have also presented a convenient method to calculate the XES or RIXS energies just by performing a *GW* calculation of a neutral ground state or of an anion without solving the Bethe–Salpeter equation, although it does not allow us to calculate the spectral intensity. The results obtained in this approach are also in good agreement with the experimental values of the XES and RIXS energies. In particular, in the case of the XES analysis, the approach treating a neutral molecule can give better results compared to the full *GW* + BSE calculation for a cation molecule with a deep core hole.

In terms of the computational scalability, the *GW* + BSE method is advantageous compared to the EOM-CCSD method if we use the generalized plasmon pole model[54] instead of doing the numerical ω integration. The EOM-CCSD calculation with the localized basis scales as N^6. On the other hand, the *GW* + BSE calculation using the reciprocal lattice space representation scales as N^4. For more precise discussion, the atomic vibration effect[24] is also important, although this is beyond the scope of the present study.

Conflicts of interest

There are no conflicts to declare.

Acknowledgements

This work was supported by the Grant-in-Aid Scientific Research B (Grant No. 21H01877) from Japan Society for the Promotion of Science (JSPS). In this research we used supercomputers at Institute for Materials Research, Tohoku University (Project No. 202012-SCKXX-0512), at Institute for Solid State Physics, University of Tokyo, and at Kyushu University (HPCI Project ID. hp210131).

References

1 H. Asakura and T. Tanaka, *Chem. Lett.*, 2021, **50**, 1075–1085.
2 P. Zimmermann, S. Peredkov, P. M. Abdala, S. DeBeer, M. Tromp, C. Müller and J. A. van Bokhoven, *Coordination Chem. Rev.*, 2020, **423**, 213466.
3 K. Siegbahn, C. Nordling, R. Fahlman, R. Nordberg, K. Hamrin, K. Hedman, G. Johansson, T. Bergmark, S. E. Karlsson, I. Lindgren and B. Lingberg, *ESCA, Atomic, Molecular and Solid State Structure Studies by Means of Electron Spectroscopy*, Nova Acta Regiae Soc. Sci. Ups., Uppsala, 1967.
4 K. Siegbahn, C. Nordling, G. Johansson, J. Hedman, P. F. Heden, K. Hamrin, U. Gelius, T. Bergmark, L. O. Werme, R. Manne and Y. Baer, *ESCA, Applied to Free Molecules*, North-Holland, Amsterdam, 1969.
5 F. de Groot, *Chem. Rev.*, 2001, **101**, 1779–1808.
6 L. J. P. Ament, M. van Veenendaal, T. P. Devereaux, J. P. Hill and J. van den Brink, *Rev. Mod. Phys.*, 2011, **83**, 705–767.
7 M. Rohlfing and S. G. Louie, *Phys. Rev. B*, 2000, **62**, 4927–4944.
8 E. Runge and E. K. U. Gross, *Phys. Rev. Lett.*, 1984, **52**, 997–1000.
9 N. A. Besley and F. A. Asmuruf, *Phys. Chem. Chem. Phys.*, 2010, **12**, 12024–12039.
10 J. E. Rubensson, N. Wassdahl, R. Brammer and J. Nordgren, *J. Electron Spectrosc. Relat. Phenom.*, 1988, **47**, 131–145.
11 N. A. Besley, *Acc. Chem. Res.*, 2020, **53**, 1306–1315.
12 N. A. Besley, *Comput. Mol. Sci.*, 2021, **11**, e1527.
13 K. Ohno, S. Ono and T. Isobe, *J. Chem. Phys.*, 2017, **146**, 084108.

14 T. Nakashima, H. Raebiger and K. Ohno, *Phys. Rev. B*, 2021, **104**, L201116.
15 Y. Zhang, S. Mukamel, M. Khalil and N. Govind, *J. Chem. Theory Comput.*, 2015, **11**, 5804.
16 I. P. E. Roper and N. A. Besley, *J. Chem. Phys.*, 2016, **144**, 114104.
17 D. R. Mortensen, G. T. Seidler, J. J. Kas, N. Govind, C. P. Schwartz, S. Pemmaraju and D. G. Prendergast, *Phys. Rev. B*, 2017, **96**, 125136.
18 A. E. A. Fouda and N. A. Besley, *Theor. Chem. Acc.*, 2018, **137**, 6.
19 V. V. da Cruz, N. Ignatova, R. C. Couto, D. A. Fedotov, D. R. Rehn, V. Savchenko, P. Norman, H. Ågren, S. Polyutov, J. Nishkanen, S. Eckert, R. M. Jay, M. Fondell, T. Schmitt, A. Pietzsch, A. Föhlisch, F. Gel'mukhanov, M. Odelius and V. Kimberg, *J. Chem. Phys.*, 2019, **150**, 234301.
20 V. V. da Cruz, S. Eckert and A. Föhlisch, *Phys. Chem. Chem. Phys.*, 2021, **23**, 1835–1848.
21 J. Vinson, T. Jach, W. T. Elam and J. D. Denlinger, *Phys. Rev. B*, 2014, **90**, 205207.
22 J. Vinson, T. Jach, M. Müller, R. Unterumsberger and B. Beckhoff, *Phys. Rev. B*, 2016, **94**, 035163.
23 T. Aoki and K. Ohno, *Phys. Rev. B*, 2019, **100**, 075149.
24 R. C. Couto, V. V. Cruz, E. Ertan, S. Eckert, M. Fondell, M. Dantz, B. Kennedy, T. Schmitt, A. Pietzsch, F. F. Guimaraes, H. Ågren, F. Gel'mukhanov, M. Odelius, V. Kimberg and A. Föhlisch, *Nat. Commun.*, 2017, **8**, 14165.
25 T. N. Pham, S. Ono and K. Ohno, *J. Chem. Phys.*, 2016, **144**, 144309.
26 L. P. Kadanoff and G. Baym, *Quantum Statistical Mechanics: Green's function Methods in Equilibrium and Nonequilibrium Problems*, Addison-Wesley, Redwood City, California, 1962, 1989.
27 L. V. Keldysh, *J. Exp. Theor. Phys.*, 1964, **47**, 1515–1527 (*Sov. Phys. JETP*, 1965, 20, 1018–1026).
28 C. D. Spataru, L. X. Benedict and S. G. Louie, *Phys. Rev. B*, 2004, **69**, 205204.
29 E. Perfetto and G. Stefanucci, *J. Phys.: Cond. Mat.*, 2018, **30**, 465901.
30 T. S. Tan, J. J. Kas and J. J. Rehr, *Phys. Rev. B*, 2021, **104**, 035144.
31 A. B. Migdal, *J. Exp. Theor. Phys.*, 1957, **32**, 399–400 (*Sov. Phys. JETP*, 1957, **5**, 333–334).
32 A. J. Layzer, *Phys. Rev.*, 1963, **129**, 897–907.
33 F. Hüser, T. Olsen and K. S. Thygesen, *Phys. Rev. B*, 2013, **87**, 235132.
34 G. Csanak, H. S. Taylor and R. Yaris, *Adv. At. Mol. Phys.*, 1971, **7**, 287–361.
35 A. Klein and R. Prange, *Phys. Rev.*, 1958, **112**, 994–1007.
36 L. Hedin and S. Lundqvist, in *Solid State Physics Vol. 23*, ed. F. Seitz, D. Turnbull and H. Ehrenreich, Academic Press, New York, 1969, pp. 1–180.
37 G. Baym and L. P. Kadanoff, *Phys. Rev.*, 1961, **124**, 287–299.
38 G. Strinati, *Nuovo Cimento*, 1988, **11**, 1–86.
39 P. Nozières, *Theory of Interacting Fermi Systems*, Westview Press, 1964, CRC Press, FL, 2018.
40 J. R. Schrieffer, *Theory of Superconductivity*, Westview Press, 1964, CRC Press, FL, 2018.
41 S. Ono, Y. Noguchi, R. Sahara, Y. Kawazoe and K. Ohno, *Comput. Phys. Commun.*, 2015, **189**, 20–30.
42 S. Ishii, S. Iwata and K. Ohno, *Mater. Trans.*, 2010, **51**, 2150–2156.
43 T. Aoki and K. Ohno, *J. Phys.: Condens. Matter*, 2018, **30**, 21LT01.
44 D. Golze, J. Wilhelm, M. J. van Setten and P. Rinke, *J. Chem. Theory Comput.*, 2018, **14**, 4856–4869.
45 P. Glans, R. E. La Villa, Y. Luo, H. Ågren and J. Nordgren, *J. Phys. B: At., Mol. Opt. Phys.*, 1994, **27**, 3399–3414.
46 J. Nordgren, H. Ågren, L. O. Werme, C. Nordling and K. Siegbahn, *J. Phys. B: Atom. Mol. Phys.*, 1976, **9**, 295–302.
47 S. Kashtanov, A. Augustsson, Y. Luo, J. H. Guo, C. Sathe, J. E. Rubensson, H. Siegbahn, J. Nordgren and H. Ågren, *Phys. Rev. B*, 2004, **69**, 024201.
48 L. Weinhardt, M. Blum, O. Fuchs, A. Benkert, F. Meyer, M. Bär, J. D. Denlinger, W. Yang, F. Reinert and C. Heske, *J. Electron. Spectrosc. Relat. Phenom.*, 2013, **188**, 111–120.
49 L. Weinhardt, A. Benkert, F. Meyer, M. Blum, R. G. Wilks, W. Yang, M. Bär and F. Reinert, *J. Chem. Phys.*, 2012, **136**, 144311.
50 A. Benkert, F. Meyer, D. Hauschild, M. Blum, W. Yang, R. G. Wilks, M. Bär, F. Reinert, C. Heske and L. Weinhardt, *J. Phys. Chem. A*, 2016, **120**, 2260.
51 E. E. Bolton, J. Chen, S. Kim, L. Han, S. He, W. Shi, V. Simonyan, Y. Sun, P. A. Thiessen, J. Wang, B. Yu, J. Zhang and S. H. Bryant, *J. Cheminformat.*, 2011, **3**, 32.
52 J. P. Perdew and A. Zunger, *Phys. Rev. B*, 1981, **23**, 5048–5079.
53 S. M. Dancoff, *Phys. Rev.*, 1950, **78**, 382–385.
54 M. S. Hybertsen and S. G. Louie, *Phys. Rev. B*, 1986, **34**, 5390–5413.
55 G. Onda, L. Reining, R. W. Godby, R. Del Sole and W. Andreoni, *Phys. Rev. Lett.*, 1985, **75**, 818–821.
56 T. Isobe, R. Kuwahara and K. Ohno, *Phys. Rev. A*, 2018, **97**, 060502(R).
57 C. Mejuto-Zaera, C. Weng, M. Romanova, S. J. Cotton, K. B. Whaley, N. M. Tubman and V. Vlcek, *J. Chem. Phys.*, 2021, **154**, 121101.